



Thermal Degradation Behavior of a New Family of Organometallic Dendrimer

Ahmad A. Joraid¹ · Rawda M. Okasha² · Mahdi A. Al-Maghrabi³ · Tarek H. Afifi² · Christian Agatemor^{4,5} · Alaa S. Abd-El-Aziz⁴

Received: 18 November 2019 / Accepted: 7 January 2020 / Published online: 13 January 2020
© Springer Science+Business Media, LLC, part of Springer Nature 2020

Abstract

Organometallic dendrimers are one of the most attractive macromolecules owing to their unique properties that derived from the combination of the metallic moieties and the remarkable architecture of the dendrimers. A new family of organoiron dendrimers has been synthesized using divergent methodology. To gain insight into the stability of these dendrimers, we investigated their thermal property using nonisothermal thermogravimetry analysis (TGA), which reveal the kinetic triplets, the pre-exponential factor, the effective activation energy and the reaction model involved in their thermal degradation. The results were obtained at heating rates of 10, 15 and 20 °C min⁻¹. Four nonisothermal methods, the Friedman, the Ozawa and Flynn and Wall, the Kissinger–Akahira–Sunose and the Minimizing were used to investigate the variation of the effective activation energy with the extent of crystallization and, hence, with temperature. In addition, the activation energy was calculated from isothermal data. The degradation mechanism follows the Avrami–Erofeev mechanism for solid-state reaction models.

✉ Ahmad A. Joraid
aaljoraid@taibahu.edu.sa

¹ Physics Department, Faculty of Science, Taibah University, Al-Madinah Al-Munawarah, Medina 30002, Saudi Arabia

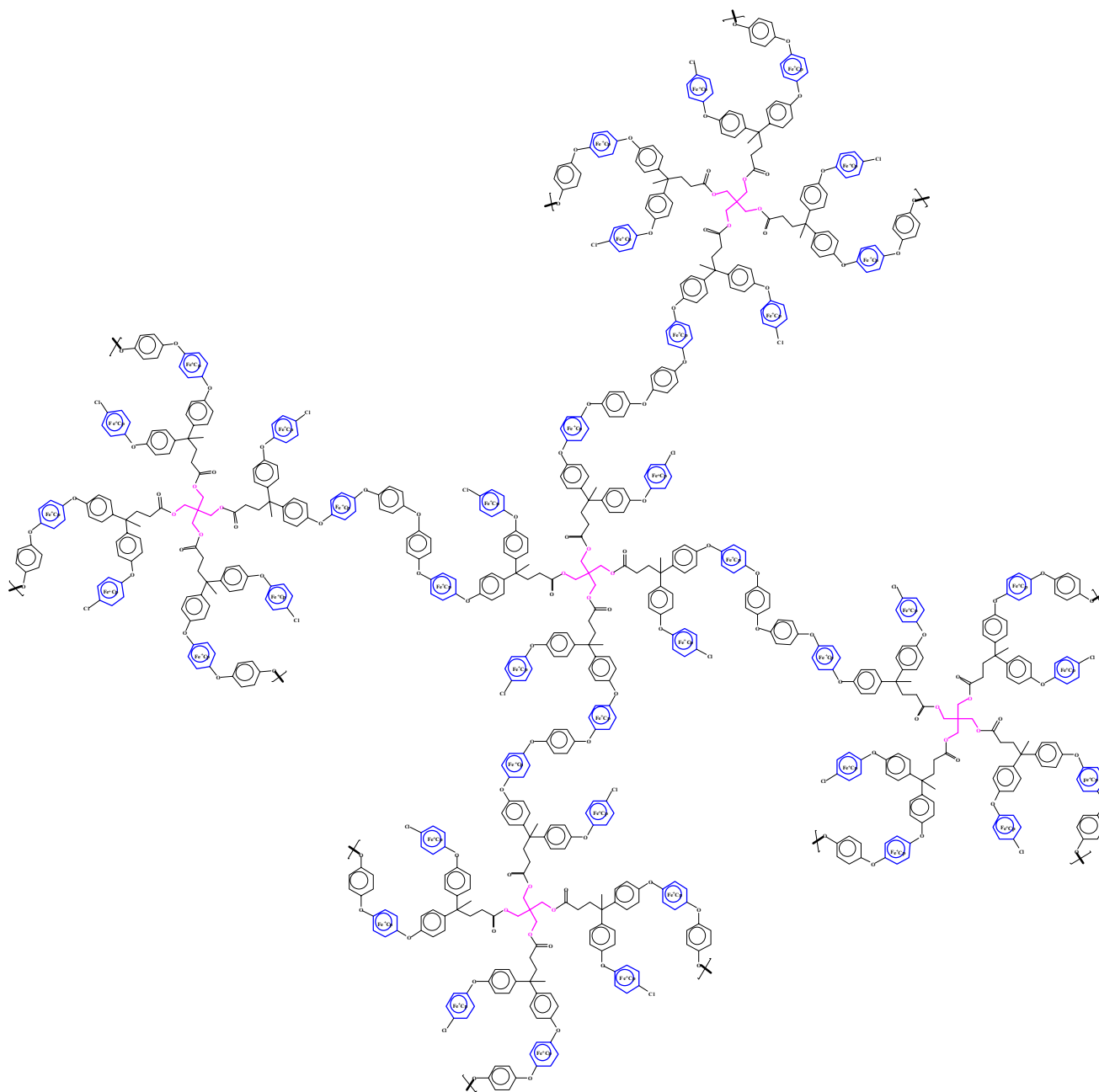
² Chemistry Department, Faculty of Science, Taibah University, Al-Madinah Al-Munawarah, Medina 30002, Saudi Arabia

³ Department of General Studies, Yanbu Industrial College, Yanbu Al-Sinaiyah, Saudi Arabia

⁴ Chemistry Department, Faculty of Science, University of Prince Edward Island, Charlottetown, Prince Edward Island C1A 4P3, Canada

⁵ Present Address: Department of Biomedical Engineering, School of Medicine, The Johns Hopkins University, Baltimore, MD 21231, USA

Graphic Abstract



Keywords Organometallic dendrimer · Thermal degradation · Kinetic · Isoconversional methods · Kinetic model

1 Introduction

Dendrimers are a unique class of macromolecules that offers the privilege of the symmetrical, monodisperse and homogeneous structure. Other remarkable features include their globular topology and tailored peripheral end groups which make dendrimers a brilliant choice in several vital

applications like biomimetic, pharmaceutical drug delivery, gene delivery, chemotherapy and diagnostic imaging. Moreover, these macromolecules have been successful candidates in supramolecular chemistry, specifically, in self-assembly processes and host–guest reactions [1–12]. In general, dendrimers have been synthesized via two protocols: a divergent route where the construction of the dendrimers is initiated at

the core and continued outward in a step-wise manner and the convergent approach that begins with the synthesis of the end groups and proceeded inwards [13–15].

The introduction of the organometallic species into dendrimer is a very attractive strategy to engineer dendrimers for desired functions. This strategy leads to the production of dendrimers macromolecules with photonic [16–21], redox [22–28] and magnetic properties [29–34]. Moreover, the concept of installing organometallic species into these macromolecules alters their catalytic, antiproliferative and sensing activities and also tunes their thermal stability. Although thermal stability plays a critical role in the processing and application of materials, our understanding of the thermal stability of organometallic dendrimers remains scanty, creating a need for a detailed investigation. Here, we designed a series of organometallic dendrimers and investigate their thermal properties using non-isothermal thermogravimetric (TG) analysis.

The theoretical basis for interpreting the thermogravimetric (TG) data, generally, provided by the classical isothermal condition of a solid-state reaction, in which the degradation fraction (the weight loss fraction) α , can be described as a function of time t according to the equation [35–42]:

$$\frac{d\alpha}{dt} = k(T)f(\alpha), \quad (1)$$

where, k is the reaction rate constant and $f(\alpha)$ is the reaction model, which describes the differential mechanism of various kinetic model functions. The reaction rate constant is usually assigned by an Arrhenius temperature dependence [35, 36, 39]:

$$k = A \exp\left(-\frac{E}{RT}\right), \quad (2)$$

where R , is the universal gas constant, E (kJ mol⁻¹) is the activation energy describing the overall of the decomposition process and A (s⁻¹) is the frequency factor. Hence, Eq. (1) will be [35, 36, 40–44]:

$$\frac{d\alpha}{dt} = A \exp\left(-\frac{E}{RT}\right)f(\alpha), \quad (3)$$

The weight loss fraction, α , can be determined from TG analysis as a fractional mass loss:

$$\alpha = \frac{m_0 - m_t}{m_0 - m_f}, \quad (4)$$

where, m_0 , m_t and m_f represent the compound mass at the onset of degradation, at any time, t and at the completion of degradation, respectively.

For non-isothermal TG kinetic study with a constant heating rate of $\beta = dT/dt$, one can get the isothermal condition

defined in Eq. (3) as temperature-dependent degradation rate as follows [35, 36, 40–42]:

$$\frac{d\alpha}{dT} = \frac{A}{\beta} \exp\left(-\frac{E}{RT}\right)f(\alpha), \quad (5)$$

The integral form of the reaction model (the reduced reaction model), $g(\alpha)$, can be obtained by integrating Eq. (5):

$$g(\alpha) = \int_0^\alpha \frac{d\alpha}{f(\alpha)} = \frac{A}{\beta} \int_{T_0}^T \exp\left(-\frac{E}{RT}\right)dT = \frac{A}{\beta} I(E, T), \quad (6)$$

To understand the reaction (degradation) model and to calculate the activation energy, various theoretical methods have been introduced. An outline of these methods used in this article is described as follows.

The Friedman method [45] directly obtained from Eq. (3), at a specific degradation fraction α and various heating rates, β_i , as:

$$\ln\left(\frac{d\alpha}{dt}\right)_{\alpha,i} = \ln[f(\alpha)A_\alpha] - \frac{E_\alpha}{RT_{\alpha,i}}, \quad (7)$$

This equation is applicable for any thermal program. For each value of the transformed part α , the activation energy E_α can be calculated from the slope of $\ln(d\alpha/dt)_{\alpha,i}$ against $1/T_{\alpha,i}$. The parameter, i , indicates the thermal program, i.e. the set temperature in isothermal experiments and the heating rate, β , in nonisothermal experiments. Since, the temperature integral Eq. (6) does not have an analytical solution, in nonisothermal experiments, hence a number of approximate solutions were provided, three of which are used in this article. First, is the Ozawa and Flynn and Wall (FWO) method [46, 47], which is measured at different, but constant, heating rates β_i .

$$\ln(\beta_i) = \ln\left(\frac{AE_\alpha}{R}\right) - \ln(g(\alpha)) - 5.3305 - 1.0518 \frac{E_\alpha}{RT_{\alpha,i}}, \quad (8)$$

The activation energy E_α can be calculated from the slope of $\ln\beta_i$ against $1/T_{\alpha,i}$. The second is the Kissinger–Aka-hira–Sunose method (KAS) [48–50] (or the generalized Kissinger method as it is sometimes called) which is given as:

$$\ln\left(\frac{\beta_i}{T_{\alpha,i}^2}\right) = \ln\left(\frac{A_\alpha R}{E_\alpha g(\alpha)}\right) - \frac{E_\alpha}{RT_{\alpha,i}}, \quad (9)$$

The activation energy E_α can be calculated from the slope of $\ln(\beta_i/T_{\alpha,i}^2)$ against $1/T_{\alpha,i}$. The third method to calculate the activation energy E_α by using isoconversional minimizing method developed by Vyazovkin [35, 48, 49]. For a set of n experiments carried out at different heating rates, β , the

activation energy, E , can be determined at any particular value of reaction progress, α , by finding the value of E_α that minimises the objective function Ω , where

$$\Omega = \sum_{i=1}^n \sum_{j \neq i}^n \frac{I(E_\alpha, T_{ai}) \beta_j}{I(E_\alpha, T_{aj}) \beta_i}, \quad (10)$$

The temperature integral, I , is given by:

$$I(E_\alpha, T_{ai}) = \int_0^{T_{ai}} \exp\left(\frac{-E_\alpha}{RT}\right) dT, \quad (11)$$

The solution of the temperature integral Eq. (6) in isothermal experiments is given by [35, 50]:

$$g(\alpha) = A \left[\exp\left(\frac{-E}{RT}\right) \right] t, \quad (12)$$

By taking the logarithm of Eq. (12) and rearranging the variables, the activation energy can be calculated at the time, $t_{\alpha,i}$, required to reach a certain value of α and temperature T_i , as:

$$\ln t_{\alpha,i} = \ln \left[\frac{g(\alpha)}{A_\alpha} \right] + \frac{E_\alpha}{RT_i}, \quad (13)$$

The activation energy for isothermal experiments, E_α in this work were calculated from the slope of $\ln t_{\alpha,i}$ vs $1/T_i$.

This study is concerned with the determination of the kinetic triplets, the pre-exponential (frequency) factor, the effective activation energy and the reaction model A , E and $f(\alpha)$ for the thermal degradation of organometallic dendrimer exemplified by a new family of cross-linked organoiron dendrimers.

2 Experimental

2.1 Materials

All chemicals and reagents were obtained from Sigma-Aldrich. Pentaerythritol, 4,4'-bis(4-hydroxyphenyl) valeric acid, potassium carbonate, ammonium hexafluorophosphate (NH_4PF_6), magnesium sulfate, N,N'-dicyclohexylcarbodiimide (DCC), 4-(dimethylamino)pyridine (DMAP), diethyl ether, acetone, chloroform, and hydrogen chloride acid were used as received. Dimethyl sulfoxide- d_6 ($\text{DMSO-}d_6$) was distilled over calcium hydride. Dimethyl sulfoxide (DMSO), N,N'-dimethylformamide (DMF) were dried, and stored over 3 Å molecular sieve before being used. Dichloromethane (DCM) was purified by passing the solvent through an Innovative Technology solvent purification system that consists of columns of alumina and copper catalyst. The synthesis of the bimetallic organoiron complex (**1**) followed previously reported procedure [1, 2].

3 Instrumentation

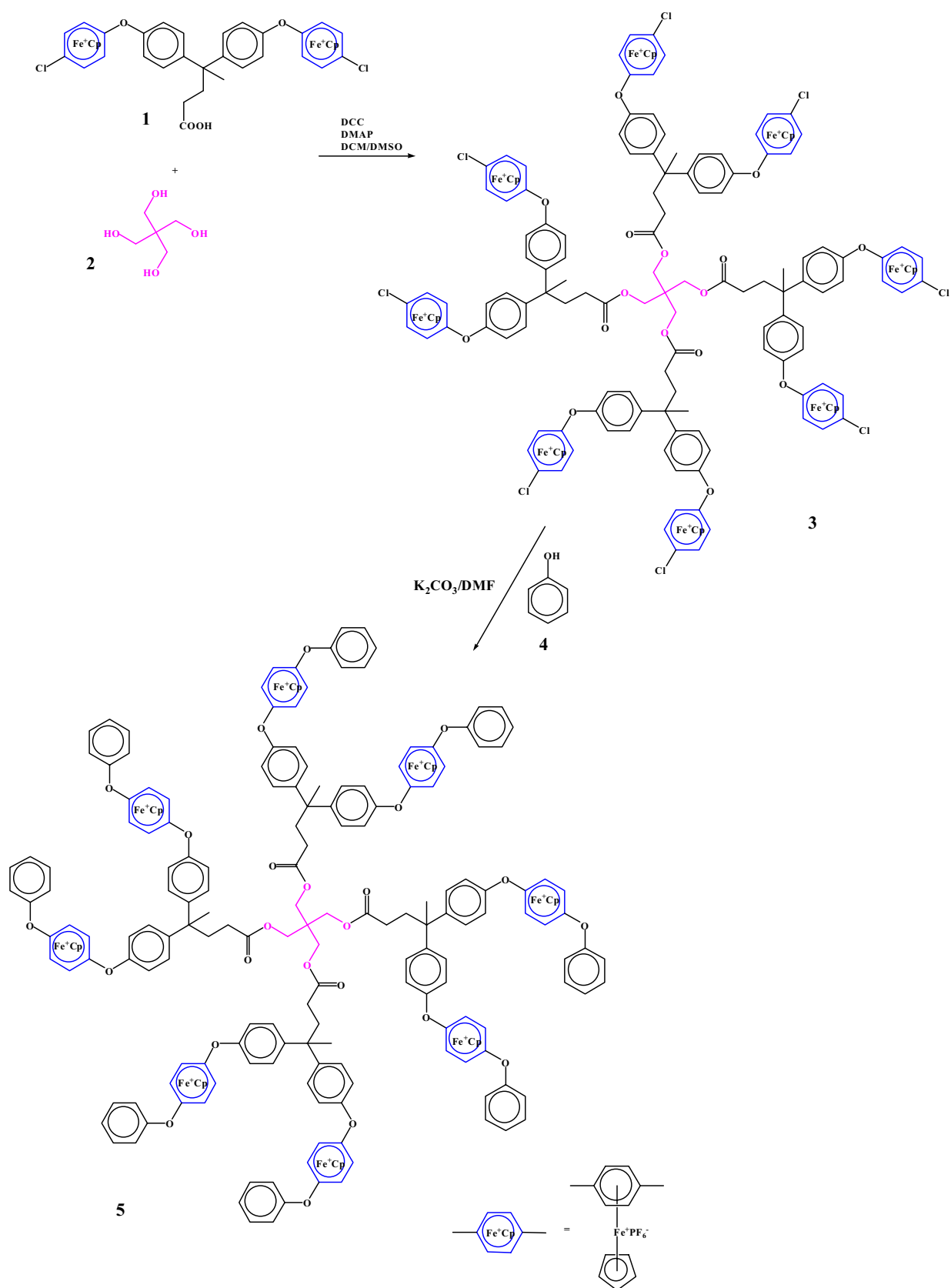
^1H - and ^{13}C -NMR spectra were recorded at 400 and 125 MHz, respectively, on a Gemini 200 NMR spectrometer, with chemical shifts calculated in Hz, referenced to solvent residues. The IR spectra of the new compounds were recorded on a Jasco FTIR-300 E Fourier Transform Infrared Spectrometer.

Thermogravimetric analysis (TGA) of the polymeric materials was carried out under nitrogen atmosphere at a heating rate of 10, 15 and 20 °C min^{-1} from room temperature to 750 °C using 3 mg of sample. The Thermogravimetric Analyzer (TGA) & Differential Scanning Calorimeter (DSC)—TA Instruments DSC SDT Q600 was used. The DSC SDT Q600 was calibrated by measuring the melting temperature and enthalpy of indium ($T_m = 429.75\text{K}$, $\Delta H_m = 28.55\text{Jg}^{-1}$) as a standard material. The advanced thermokinetics software package AKTS—Thermokinetics, Ver. 4.15, was used for all kinetics analysis in this study.

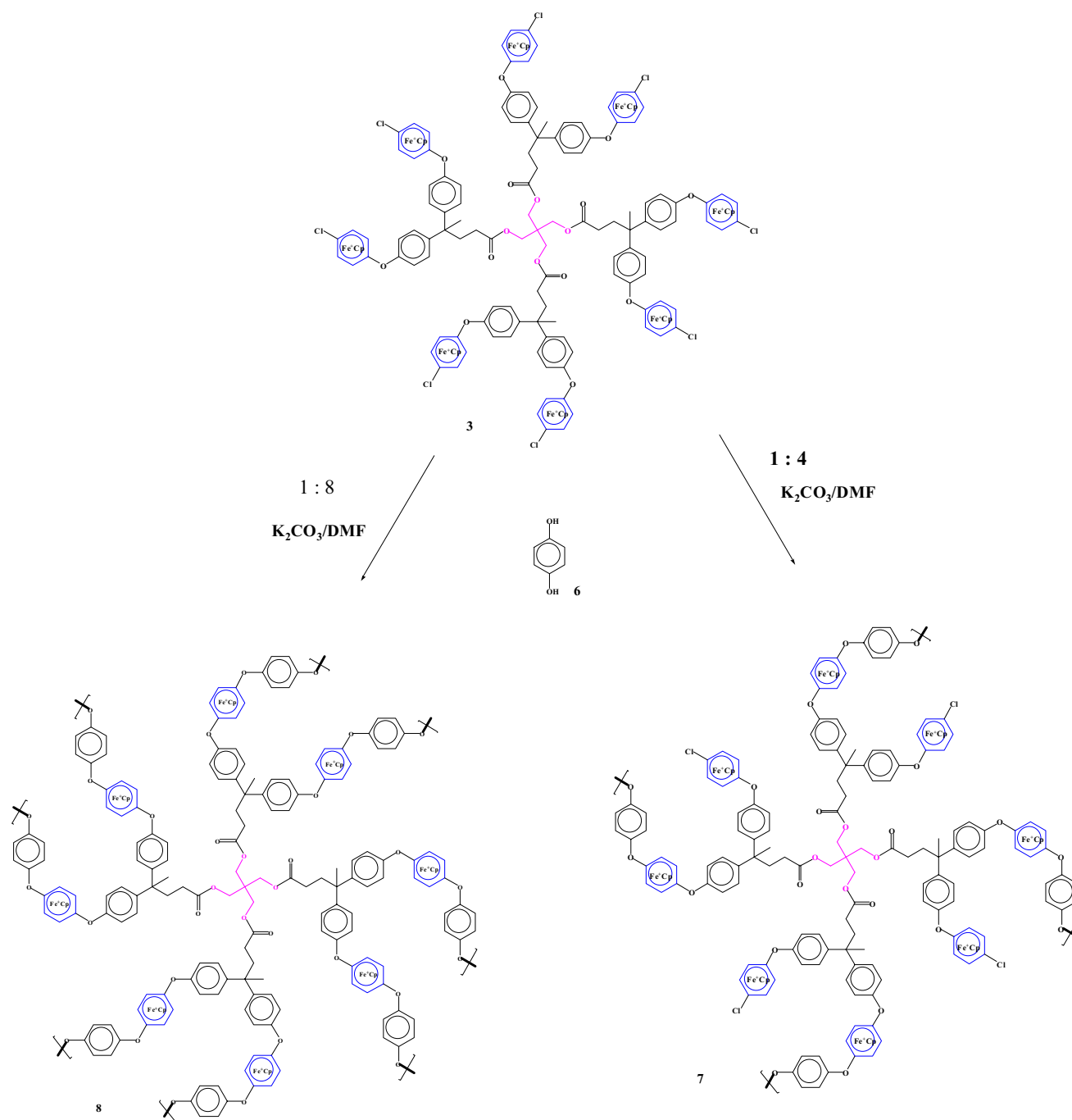
4 Synthesis Phenol-Terminated G_0 Dendrimer (**5**)

Dendrimer **5** has been synthesized in two steps procedure. The first step encompasses Steglich esterification of the bimetallic complex **1** with pentaerythritol core in order to isolate G_0 dendrimer **3**. A 50 mL round-bottom flask was charged with pentaerythritol **2** (0.170 g, 1.27 mmol), **1** (5.28 g, 5.08 mmol), DMAP (0.500 g, 4.08 mmol), 10 mL of 3:1 DCM:DMSO solution. The solution was stirred and cooled in an ice bath to 0 °C under nitrogen atmosphere while DCC (1.15 g, 5.59 mmol) was added over a 5-min period. The ice-bath was removed after 5 min and the reaction mixture stirred under nitrogen for 3 h at room temperature. Precipitated dicyclohexylurea (DCU) was removed by filtration through a Büchner funnel and the filtrate was hydrolyzed in 50 mL of ice water to which NH_4PF_6 (1.66 g, 10.2 mmol) was added. The product was extracted with three 50-mL portions of 5:1 DCM/DMF mixture. The extracts were washed with two 50-mL portions of 5% HCl and subsequently with two 50-mL portions of sodium bicarbonate, dried over MgSO_4 , filtered, and the solvent removed with a rotary evaporator. The crude product of **3** was dissolved in acetone, cooled to -25 °C in a freezer for 1 h, filtered to remove more DCU and precipitated from diethyl ether. The resulting yellow-green solid, **3**, was collected by suction filtration and dried under vacuum at room temperature.

The synthesis of dendrimer **5** followed a well-established chemistry [3]. A 50-mL round-bottom flask was charged with phenol (**4**) (0.76 g, 8.04 mmol), **3** (4.22 g, 1.00 mmol),



Scheme 1 Synthesis of dendrimer 5



Scheme 2 Synthesis of dendrimers **7** and **8**

K_2CO_3 (4.87 g, 35.3 mmol), and 10 mL of DMF. The reaction mixture was stirred at room temperature for 16 h after flushing with nitrogen for 1 h. Subsequently, the reaction mixture was poured into 300 mL of 10% HCl solution, and NH_4PF_6 (1.66 g, 10.2 mmol) was added to precipitate the product. The product was filtered and dried under vacuum. Yield: (4.14 g, 93%). 1H NMR data (400 MHz; DMSO- d_6 , δ): 7.55 (8H, br. s, uncomplexed Ar H), 7.33 (24H, br. s,

uncomplexed Ar H & phenyl Ar H), 7.23 (13H, br. s, uncomplexed Ar H & phenyl Ar H), 6.99–7.04 (16H, m, uncomplexed Ar H), 6.27 (8H, br s, complexed Ar H), 5.22 (40, s, Cp H), 4.01 (8H, br s, CH_2), 2.48 (8H, br s, CH_2), 2.04 (8H, br s, CH_2), 1.61 (12H, s, CH_3); ^{13}C NMR (125 MHz, DMSO- d_6 , δ): 174.6 (C=O), 157.1, 130.5, 129.9, 129.6, 128.9, 128.3, 126.0, 120.2, 119.6, 117.3, 74.9, 74.6 (Ar C), 77.6 (Cp C), 45.1 (quat C), 35.8, 29.5 (CH_2), 26.7 (CH_3).

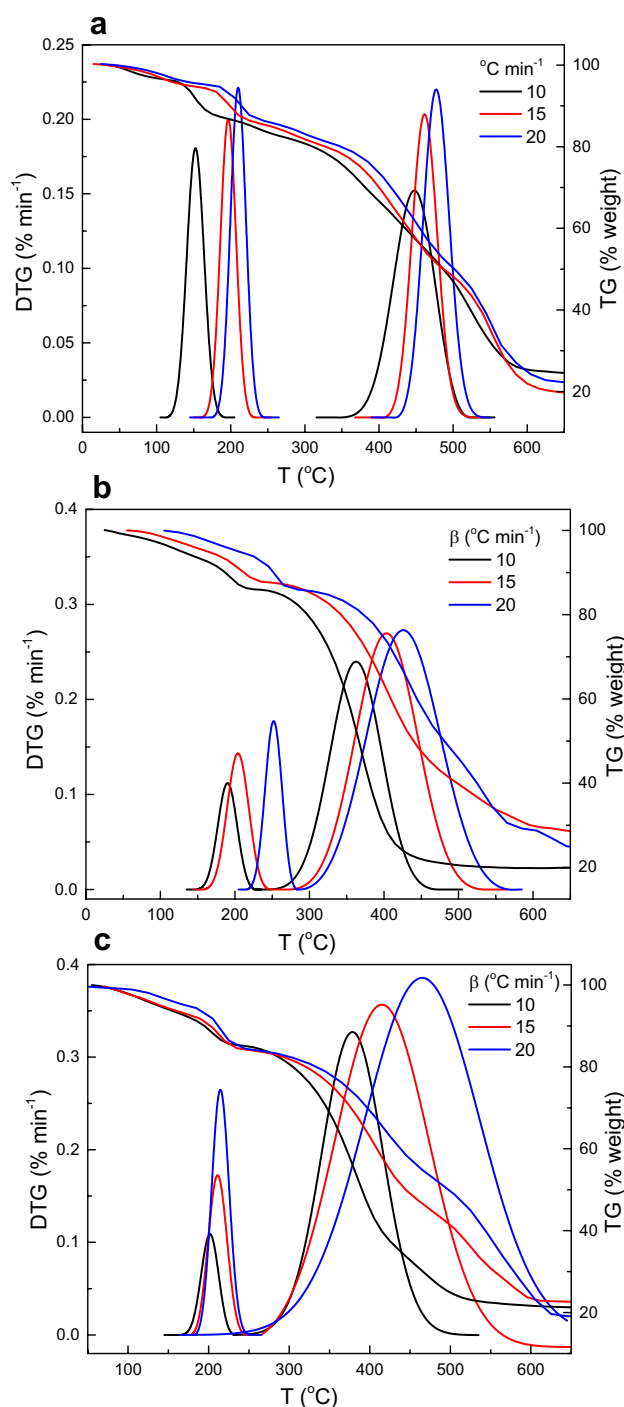


Fig. 1 a–c. TG and DTG curves of **a** dendrimer 5, **b** dendrimer 7 and **c** dendrimer 8 at heating rates 10, 15 and 20 °C min⁻¹

ATR-FIIR: $\nu_{\max}/\text{cm}^{-1}$ 3457 (COOH), 2968 (Cp-CH), 1719 (CO), 1220 (C–O–C).

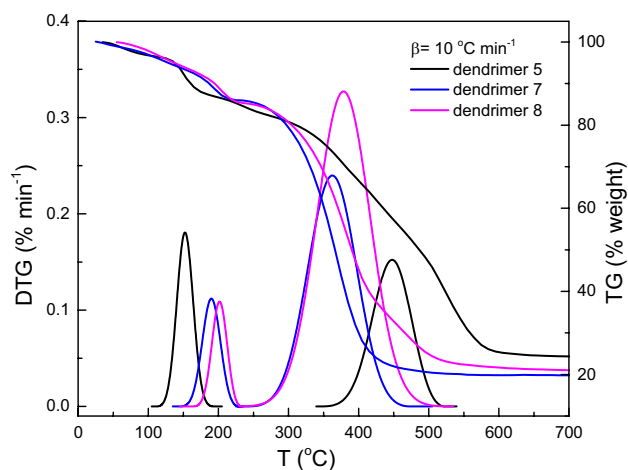


Fig. 2 Comparison of TG and DTG curves of dendrimer 5, dendrimer 7 and dendrimer 8 at heating rates 10 °C min⁻¹

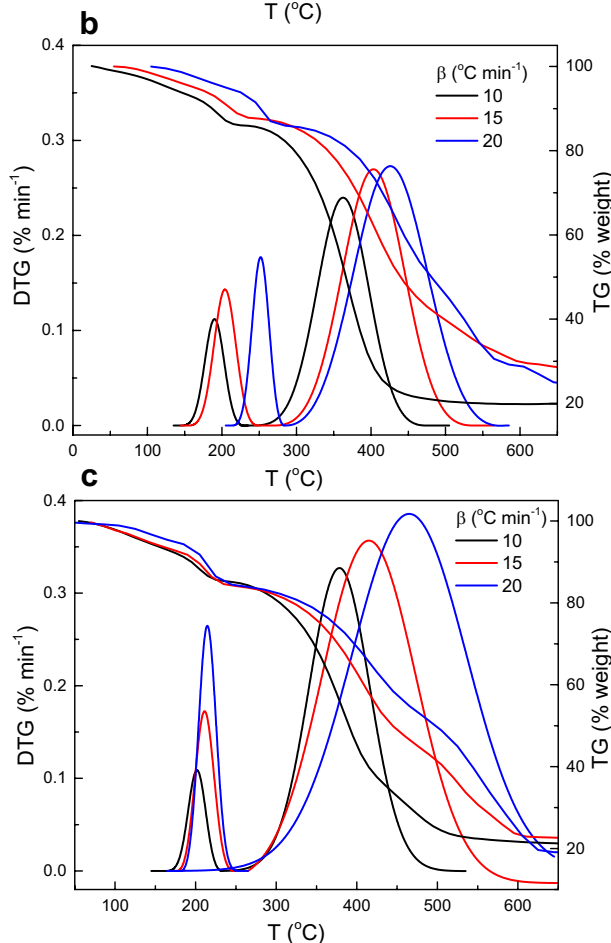


Fig. 3 Degree of conversion, α , as a function of temperature at different heating rates for the two steps of degradation LTD and HTD

5 Synthesis of Crosslinked G0 Dendrimers (7 & 8)

In a procedure analogous to the synthesis of **5**, dendrimers **7** & **8** were synthesized via the reaction of G0 dendrimer **3** (4.22 g, 1.00 mmol) and hydroquinone **6** with molar ratio 1:4 to isolate dendrimer **7** and ratio 1:8 to produce dendrimer **8**. The reactions were performed at room temperature for 16 h after flushing with nitrogen for 1 h in the presence of K_2CO_3 (4.87 g, 35.3 mmol), and 10 mL of DMF. The reaction mixture was then poured into 300 mL of 10% HCl solution, and NH_4PF_6 (1.66 g, 10.2 mmol) was added to precipitate the product. The product was filtered and dried under vacuum.

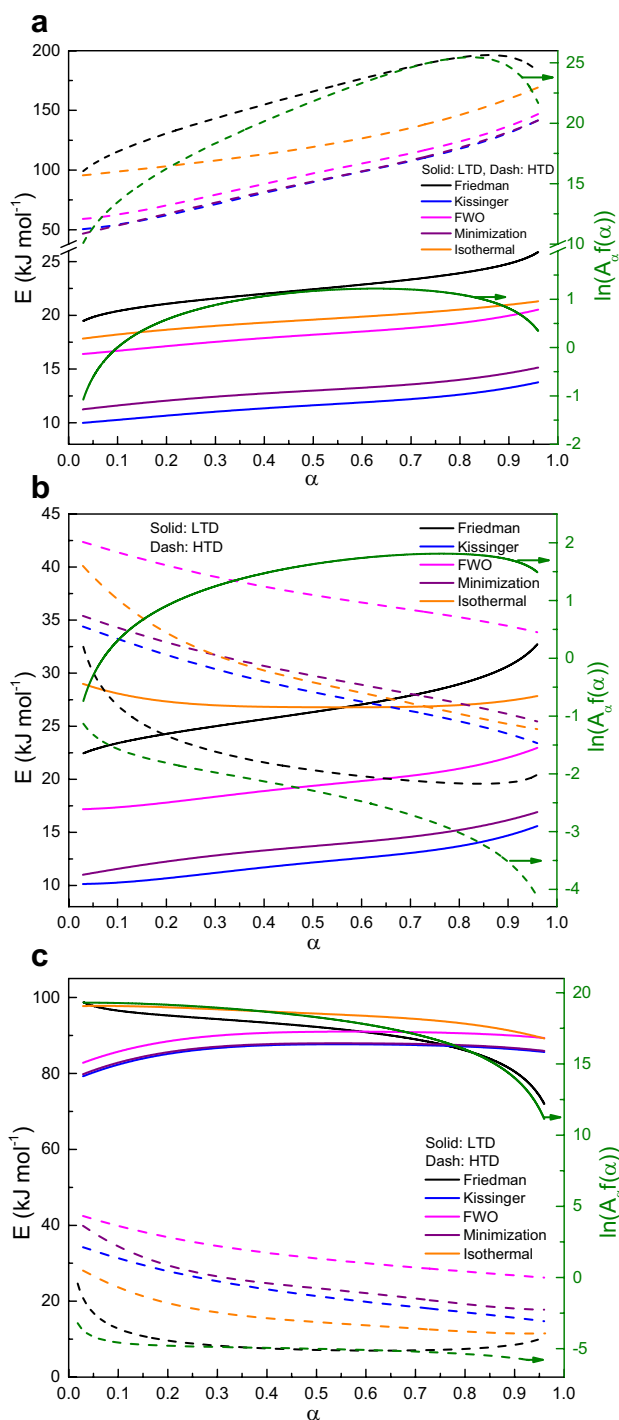


Fig. 4 a–c. Dependence of the activation energy of degradation E_{α} and of the experimental $\ln(A_{\alpha} f(\alpha))$ values on the extent of decomposition α , **a** dendrimer 5, **b** dendrimer 7 and **c** dendrimer 8

Dendrimer 7, Yield: (84 mg, 82%). ^1H NMR data (400 MHz, DMSO-d_6 , δ): 7.15 (32H, br s, uncomplexed Ar H & hydroquinone Ar H), 6.93 (16H, br s, uncomplexed Ar H), 6.17 (32H, br s, complexed Ar H), 5.19 (40H, s, Cp H), 4.02 (8H, br s, CH_2), 2.36 (8H, br s, CH_2), 2.09 (8H,

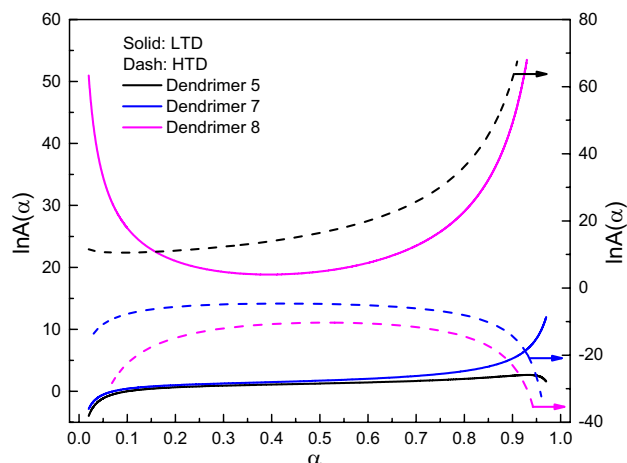


Fig. 5 The dependence of logarithm of the experimental pre-exponential frequency, $\ln(A(\alpha))$, on the degradation fraction, α , for the three dendrimers

br s, CH_2), 1.60 (12H, br s, CH_3); ^{13}C NMR (125 MHz, DMSO-d_6 , δ): 172.5 (C=O), 155.6, 154.2, 144.6, 131.5, 129.8, 129.1, 122.0, 119.8, 116.8, 75.1, 73.6 (Ar C), 77.7 (Cp C), 61.9 (CH_2), 44.8 (quat C), 35.9, 29.7 (CH_2), 26.9 (CH_3). ATR-FIIR: $\nu_{\text{max}}/\text{cm}^{-1}$ 2925 (Cp CH), 1724 (CO), 1220 (C–O–C).

Dendrimer 8, Yield: (84 mg, 82%). ^1H NMR data (400 MHz, DMSO-d_6 , δ): 7.15 (48H, br s, uncomplexed Ar H & hydroquinone Ar H), 6.92 (16H, br s, uncomplexed Ar H), 6.16 (32H, br s, complexed Ar H), 5.18 (40H, s, Cp H), 4.00 (8H, br s, CH_2), 2.36 (8H, br s, CH_2), 2.07 (8H, br s, CH_2), 1.59 (12H, br s, CH_3); ^{13}C NMR (125 MHz, DMSO-d_6 , δ): 172.5 (C=O), 155.8, 154.2, 144.6, 131.5,

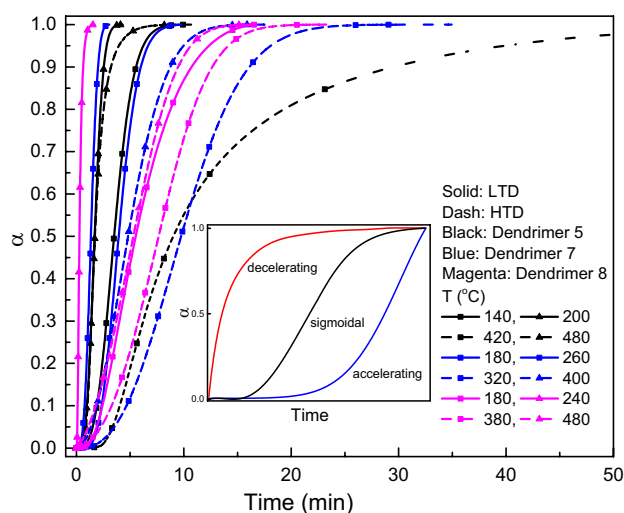


Fig. 6 Examples of the predicted isothermal degradation fractions α for the three samples under investigation. The inset figure represents the characteristic α vs t reaction profile

129.8, 129.1, 122.0, 119.8, 116.8, 74.8, 73.4 (Ar C), 77.4 (Cp C), 61.7 (CH₂), 44.8 (quat C), 35.9, 29.5 (CH₂), 26.6 (CH₃). ATR-FIIR: $\nu_{\max}/\text{cm}^{-1}$ 2924 (Cp CH), 1723 (CO), 1219 (C–O–C).

6 Results and Discussion

The synthesis of the three dendrimers was accomplished via a divergent pathway. A condensation reaction of the pentaerythritol core with valeric bimetallic complex **1** in the presence of a catalytic amount of dimethyl amino pyridine (DMAP) and dicyclohexyl carbodiimide (DCC) resulted in the formation of dendrimer **3**, where the peripheral groups were then capped with phenol molecules to form dendrimer **5**, Scheme 1.

Dendrimers **7** and **8** were obtained by the reaction of complex **3** with different ratio of the hydroquinone compound. Dendrimer **7** was obtained with ratio 1:4 while ratio 1:8 led to the formation of dendrimer **8**, Scheme 2. Due to the bifunctionality of the hydroquinone as well as the high reactivity of the chloride on the complexed arenes, these dendrimers have a high possibility of crosslinking. Scheme 3 depicts this crosslinking behavior.

7 Thermal Behavior

Characterization of materials and their response to temperature is very important to determine their thermal stability. Dendrimers are a class of material that has interested features, which made it a very good option in different applications such as flat panel display. So, understanding their thermal stability is a crucial to determining their processing parameters as well as their applications. Thermal stability and thermal degradation can be explored through a variety of techniques. Thermogravimetric analysis (TGA) is the most commonly used technique to measure the relative weight change versus temperature in a controlled atmosphere. More insight can be obtained by measuring the change in mass as a function of time under isothermal and non-isothermal conditions.

Figure 1a–c presents the thermogravimetric (TG) curves and derivative thermogravimetric (DTG) curves obtained for the three samples depicted in Schemes 1 and 2. The samples were heated from room temperature to 700 °C at heating rate of 10, 15 and 20 °C min⁻¹. The mass-loss curves shows that the degradation process can be divided into two distinguished regimes. For heating rate of 10 °C min⁻¹, the low temperature degradation (LTD) regime for dendrimer 5, dendrimer 7 and dendrimer 8 occurring at about 131–187, 167–215 and 184–231 °C, respectively and accompanied by about 15% loss. In addition, the high temperature

degradation (HTD) regime occurring at about 304–589, 269–472 and 285–542 °C for Dendrimer 5, Dendrimer 7 and Dendrimer 8, respectively and accompanied by about 60% loss. The amount of residual mass after the full degradation ranges from 20 to 25%. However, Dendrimer 7 and Dendrimer 8 show the maximum lost in which residual mass reaches 10% at the 650 °C.

Figure 2 shows that in Dendrimer 7 and Dendrimer 8, the second degradation peaks were more pronounced and occurred at lower temperature than Dendrimer 5, suggesting the lower thermal stability at temperature range 300 °C and beyond. Figure 2 shows clearly that for the first degradation of Dendrimer 5 occurred at about 131 °C, which can be attributed to the loss of cyclopentadienyl iron(II) moiety attached to the terminals of the structure [51]. The first degradation for Dendrimer 7 and Dendrimer 8 occurred at about 167 and 184 °C, respectively, for heating rate of 10 °C min⁻¹, which is a higher temperature compared to dendrimer 5. Such increase in the degradation temperature, compared to dendrimer 5, can be explained in the basis of number of cationic iron centers, which cause a delay of the first degradation of dendrimer 7 and dendrimer 8.

In the same manner, the temperature progress of all the three samples showed a second degradation stage occurring at different temperatures. For the heating rate of 10 °C min⁻¹, the second degradation occurred at about 304, 269 and 285 °C for dendrimer 5, dendrimer 7 and dendrimer 8, respectively. Such high temperature for dendrimer 5 can be ascribed to the breakage of the dendritic backbone and the presence of phenolic peripheral groups, indicating the higher thermal stability of such structure compared to dendrimer 7 and dendrimer 8. On the other hand, the existence of activated chloride terminal, which is considered as a good leaving group, can be responsible for decreasing the thermal stability of dendrimer 7 as such leaving group can form a free radical that might accelerate the degradation of the dendritic unit. Our observation suggests that dendrimer 8 shows a moderate behavior. Such behavior can be explained in the basis of the possible crosslinking that in this sample. Figure 3 presents the reaction progress as a function of temperature for the three prepared samples. As observed in the figure, the first degradation occurs at low temperatures. However, as the temperature increases, the second patch of curves related to the second degradation appears at higher range of temperatures, which is consistent with the degradation peaks presented in Fig. 1.

Previously, stated, that the Friedman Eq. (7), the Ozawa and Flynn and Wall (FWO) Eq. (8), the Kissinger–Akahira–Sunose (KAS) Eq. (9) and the Minimizing (Vyazovkin) Eq. (10) methods were used to investigate the variation of the effective activation energy with the extent of degradation and, hence, with temperature. In addition, the activation energy was calculated from isothermal data Eq. (13).

Fig. 7 a–c. The plots of $\ln(d\alpha/dt)_{\alpha,i}$ vs. $1/T_{\alpha,i}$, $\ln\beta_i$ vs. $1/T_{\alpha,i}$, $\ln(\beta_i/T_{\alpha,i}^2)$ vs. $1/T_{\alpha,i}$ and $\ln t_{\alpha,i}$ vs. $1/T_{\alpha,i}$ and a straight regression lines for the three samples used

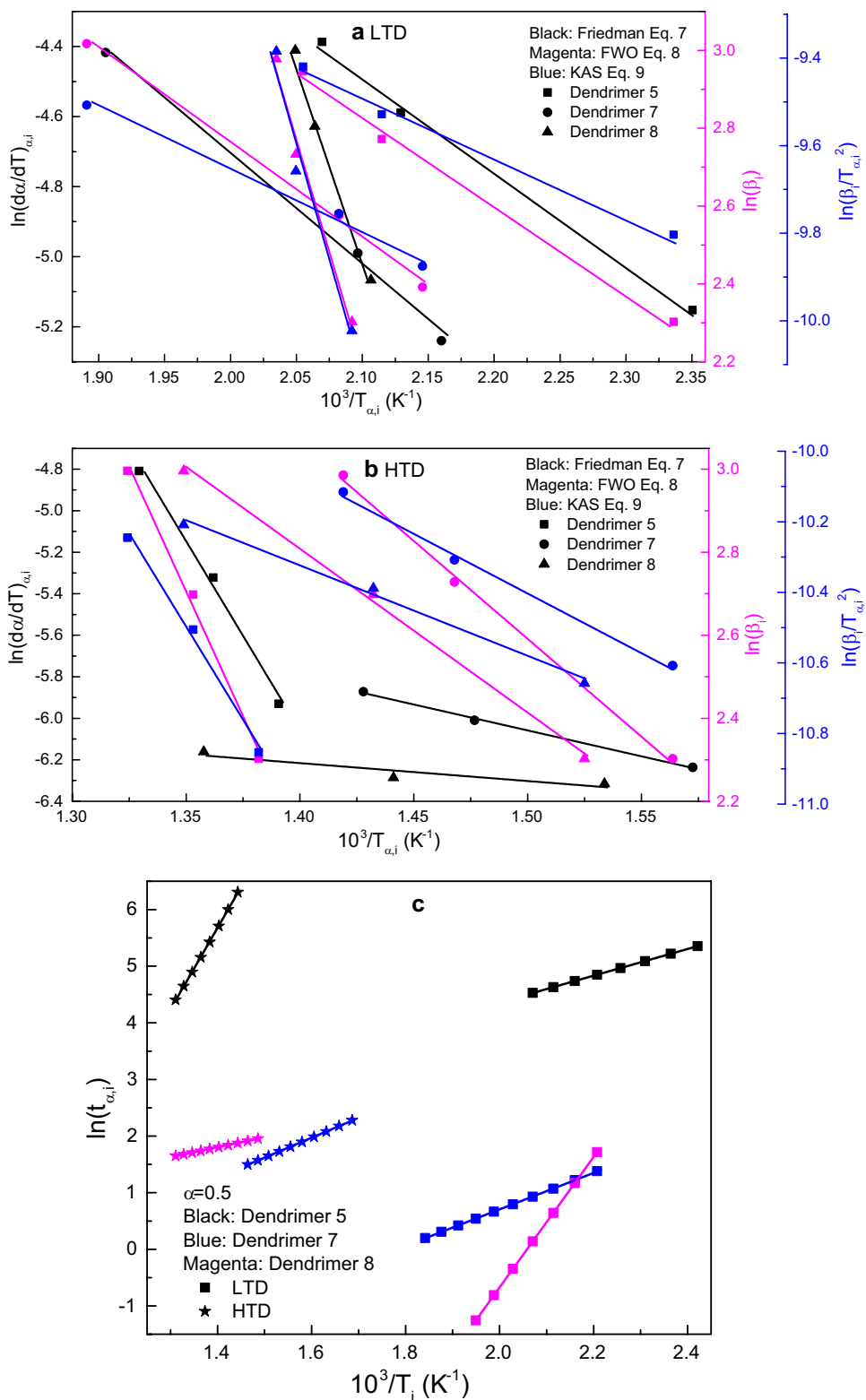


Figure 4a–c summarizes the calculated activation energies for the three different samples using Friedman, FWO, KAS and minimizing methods as a function of conversion fraction, α . Correspondingly, this figure shows the variation of

$\ln(A_w f(\alpha))$. The dependence of $\ln A(\alpha)$ on α for the three samples investigated is shown in Fig. 5, more or less, this dependence is typically as the dependence of $E(\alpha)$ on α . By using the AKTS-Thermokinetics software the nonisothermal

Table 1 Comparison of the values of the activation energy for the samples under investigation

| Method | Dendrimer 5 | | Dendrimer 7 | | Dendrimer 8 | |
|-------------------|--------------------------------------|--------------------------------------|--------------------------------------|--------------------------------------|--------------------------------------|--------------------------------------|
| | $E(\text{LTD})$ kJ mol ⁻¹ | $E(\text{HTD})$ kJ mol ⁻¹ | $E(\text{LTD})$ kJ mol ⁻¹ | $E(\text{HTD})$ kJ mol ⁻¹ | $E(\text{LTD})$ kJ mol ⁻¹ | $E(\text{HTD})$ kJ mol ⁻¹ |
| Friedman Eq. 7 | 22.4 | 151.7 | 26.3 | 20.8 | 92.6 | 7.2 |
| FWO Eq. 8 | 18.1 | 95 | 19.3 | 37.2 | 91.2 | 31.2 |
| KAS Eq. 9 | 11.6 | 87.7 | 12.1 | 28.1 | 87.9 | 21.3 |
| Isothermal Eq. 13 | 19.6 | 19.4 | 26.8 | 29.1 | 95.8 | 14.5 |

kinetic parameters E_α and $\ln(A_\alpha f(\alpha))$ can be used to predict the variation of the conversion degree versus time for a given temperature, which is known as isothermal kinetic predictions [52–56]. An example of the prediction of the isothermal conversion fraction for the three samples under investigation is shown in Fig. 6. From this figure and by applying Eq. 13, the activation energy under isothermal condition was obtained. The calculated values are shown in Fig. 4 contemporary with nonisothermal results.

Figure 4a presents the activation energy for degradation E_α resulted the degradation of dendrimer 5. The plot of E_α revealed a clear difference between the two steps (LTD and HTD) with respect to the conversion fraction α . The variation of E_α is particularly independent of the value of α for LTD step, while, for HTD step the activation energy is much higher than LTD step and somewhat, it increases with α . This increase might be attributed to the higher energy barrier of Dendrimer 5 which requires more energy to overcome. Such high activation energy agrees well our observation where Dendrimer 5 has shown the higher thermal stability compared to the other samples. A noticeable change in activation energy behavior for Dendrimer 7 was observed as shown in Fig. 4b. This sample shows that the values of the activation energy for degradation are almost in the same range for the two steps LTD and HTD. The activation energy decreases with α for HTD step. However, Dendrimer 8 shows considerable larger values of the activation energy E_α for LTD step than HTD step as shown in Fig. 4c. The variation of E_α for both steps is mainly independent on α .

To conclude the activation energy E , dependence on the compounds, Friedman, FWO and KAS Eqs. (7), (8) and (9), as well the isothermal Eq. (13) were used on a conversion range of $\alpha = 0.5$. The plots of $\ln(d\alpha/dt)_{\alpha,i}$ vs. $1/T_{\alpha,i}$, $\ln\beta_i$ vs. $1/T_{\alpha,i}$, $\ln(\beta_i/T_{\alpha,i}^2)$ vs. $1/T_{\alpha,i}$ and $\ln t_{\alpha,i}$ vs. $1/T_{\alpha,i}$ are shown in Fig. 7a–c, the straight lines are linear fittings according to the mentioned equations. From this figure, the values for the activation energy are summarized in Table 1.

Figure 8a–c displays the resulting $E_\alpha(T)$ dependence; all values are positive, which simply indicate that the degradation rate increases with increases temperature. The mathematical reaction model $f(\alpha)$ was used to describe the degradation process more precisely and to decide which one of the

solid-state kinetic models [35] can be used for the process. The first step to describe $f(\alpha)$ is by using the characteristic $\alpha(t)$ reaction profile [35] shown in Fig. 6 as inset figure. The curves in this figure clearly, implies a sigmoidal model. The Avrami–Erofeev equation exemplified this type of model.

$$f(\alpha) = n(1 - \alpha)[- \ln(1 - \alpha)]^{\frac{(n-1)}{n}}, \quad (14)$$

Moreover, the integral form is,

$$g(\alpha) = [- \ln(1 - \alpha)]^{\frac{1}{n}}, \quad (15)$$

where n is a constant (the Avrami exponent).

The integral form of the reaction model, $g(\alpha)$, is normally used to describe the kinetics of phase transformation in solids [35, 38, 44, 56]. The calculated kinetic function, $g(\alpha)$, using nonisothermal experimental data is shown in Fig. 9a–c for all three samples. The solid line was calculated according to the Avrami–Erofeev models A1.5, A2, A3 and A4, which take the Avrami number n equal to 1.5, 2, 3 and 4, respectively. Comparison between the experimental results and the theoretical models provided information about the degradation mechanism during the course of transformation. Undoubtedly, it is very clear from Fig. 9a–c that the degradation for all three samples follow an Avrami–Erofeev mechanism in the 10–20 K min⁻¹ heating rate ranges. However, from Fig. 9a the analysis clearly indicates a change in mechanism for Dendrimer 5 with a change in the heating rate for both steps LTD and HTD. This change suggests that n increases with increasing heating rate for both steps. The experimental analysis indicates that Dendrimer 5(LTD) follows A1.7 at low heating rate of $\beta = 10$ °C min⁻¹, and comes close to A2.56 at heating rate of $\beta = 20$ °C min⁻¹. Though, Dendrimer 5 (HTD) follows A2.15 and A3.56 for heating rates $\beta = 10$ and 20 °C min⁻¹, respectively. On the other hand, and for Dendrimer 7 (LTD) the solid-state reaction model $g(\alpha)$ changes from A1.9 toward A2.93 as the heating rate goes up. While, for the high step (HTD), $g(\alpha)$ is very nearly constant with a minor decrease from A1.38 to A1.2 as the heating rate increases from $\beta = 10$ and 20 °C min⁻¹. The solid-state reaction mechanism for dendrimer 8 (LTD) closely follows A2 for $\alpha > 0.4$, with a divergence toward

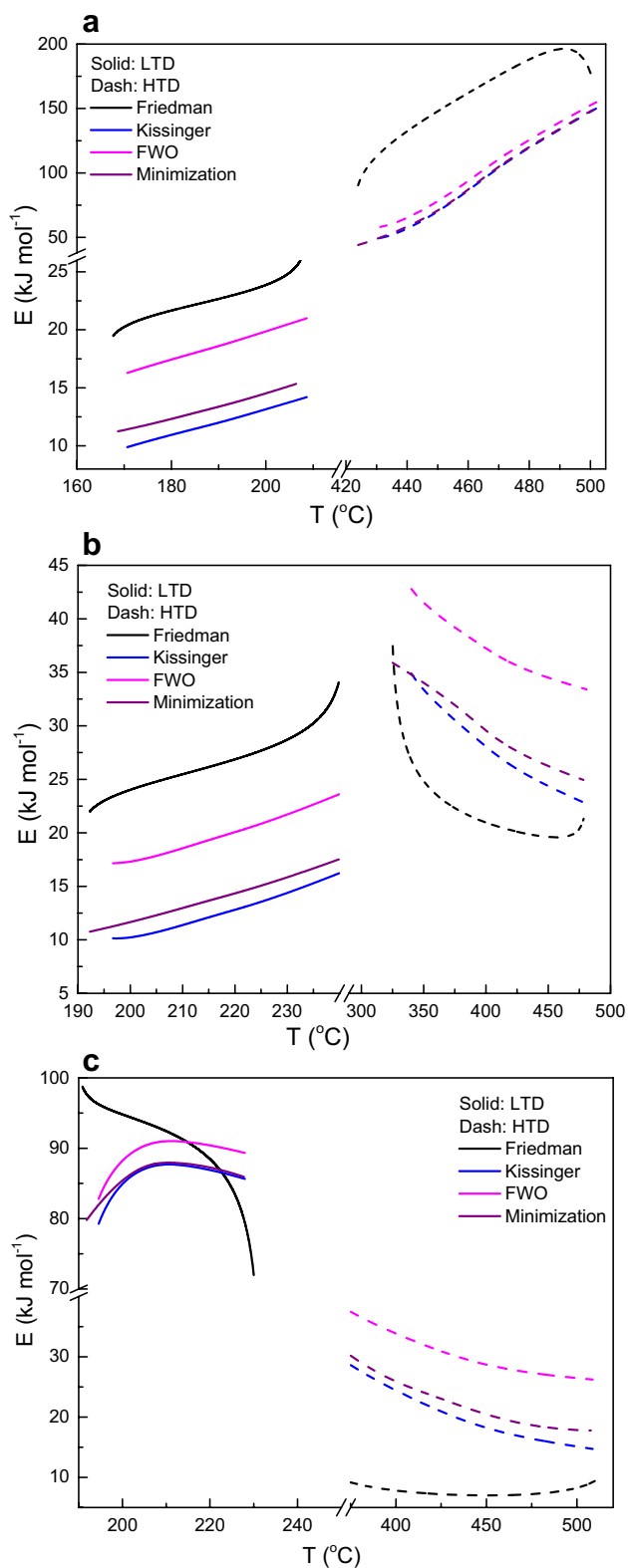


Fig. 8 a–c. Dependence of the activation energy of degradation E_α on the extent of degradation α , **a** dendrimer 5, **b** dendrimer 7 and **c** dendrimer 8

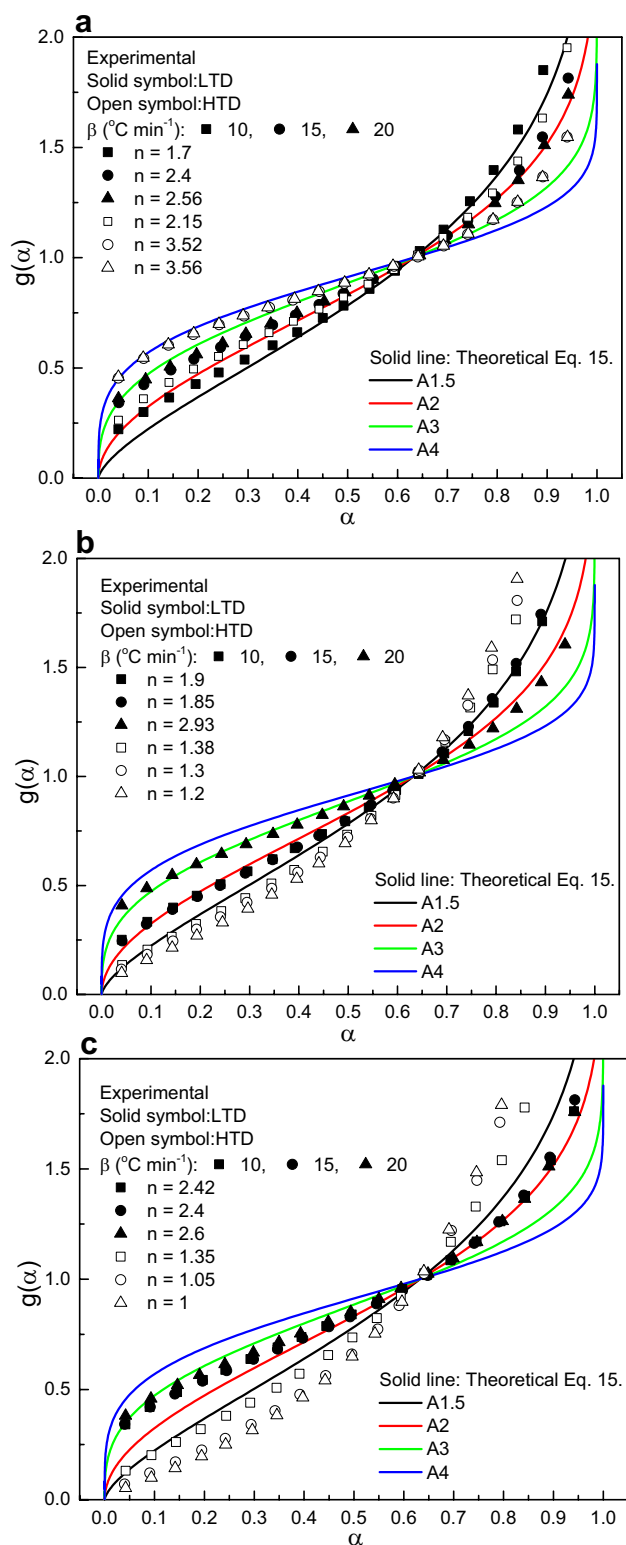


Fig. 9 a–c. The variation of the reduced reaction model, $g(\alpha)$, versus degradation fraction, α , the solid line was calculated from the Avrami–Erofeev mechanism. **a** dendrimer 5, **b** dendrimer 7 and **c** dendrimer 8

a higher values of $g(\alpha)$ at the initial stage of degradation

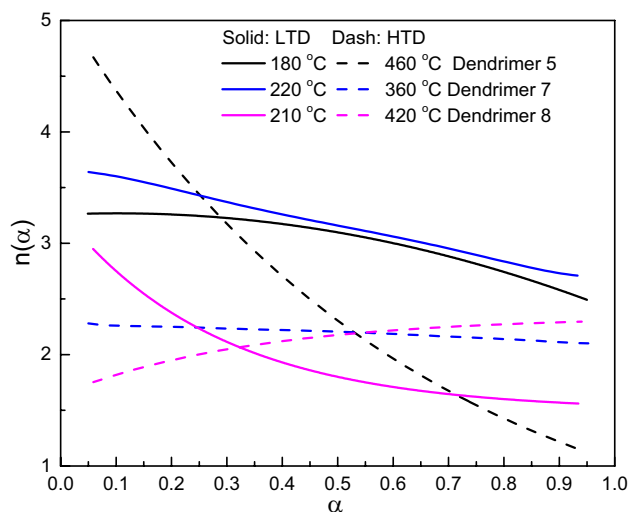


Fig. 10 Local Avrami exponent $n(\alpha)$ versus the degradation fraction α at different temperatures

($\alpha > 0.4$). Nevertheless, the solid-state reaction model $g(\alpha)$ for high step of dendrimer 8 (HTD), takes almost the same behavior as dendrimer 7 (HTD), with a minor decrease from A1.35 to A1 as the heating rate increases from $\beta = 10$ and $20 \text{ }^\circ\text{C min}^{-1}$.

Finally, the local Avrami exponent, $n(\alpha)$, gives more details about the degradation process. The local Avrami exponent is given by [56]:

$$n(\alpha) = \frac{\partial \ln [-\ln (1 - \alpha_t)]}{\partial \ln t} \quad (16)$$

The values of $n(\alpha)$ at certain temperatures as a function of degradation fraction α are shown in Fig. 10 for the three samples under investigation. For dendrimer 5 and dendrimer 7 (LTD) $n(\alpha)$ slightly decreases with the development of degradation and lies between 3.2–2.5 and 3.6–2.7, respectively. These isothermal results agree with $g(\alpha)$ obtained from nonisothermal data, which are shown in Fig. 9a and b, where $g(\alpha)$ also shifts to a lower A's value with the development of degradation process. $n(\alpha)$ proceeds with the same behavior i.e. decreases as α increases, but with lower values between 2.9 and 1.6, which is also agree with $g(\alpha)$ shown in Fig. 9c, where $g(\alpha)$ shifts from about A3 towards A2 with increasing α . However, for dendrimer 5(HTD) a dramatic change was realized in the variation of the local Avrami exponent $n(\alpha)$. It strongly decreased with the development of crystallization and lies between 4.7 and 1.2. For dendrimer 7 (HTD) the local Avrami exponent can almost be assumed to be constant with the development of degradation and its value about 2.2. On the other hand, for dendrimer 8 (HTD), $n(\alpha)$ slightly increases along with the development of degradation with value in the range of 1.8–2.3.

8 Conclusion

The present work describes the thermal property of a new family of organometallic dendrimers. The kinetic parameters of the organoiron dendrimers under nonisothermal conditions and predicted isothermal conditions were obtained by using TGA. The results show that the degradation process for all three compounds studied divided into two distinguished regimes. Low temperature degradation (LTD) regime occurring at about 131–231 accompanied by about 15% loss. The high temperature degradation (HTD) regime occurring at about 269–589 and accompanied by about 60% loss. The variation of the effective activation energy with the extent of degradation were investigated, by using two major isoconversional methods, differential (Friedman) method and Integral of the Ozawa and Flynn and Wall, the Kissinger–Akahira–Sunose and the Minimizing (Vyazovkin) methods. Moreover, the activation energy was calculated from isothermal results. The effect of temperature on the activation energy was investigated. Remarkable difference of activation energy behavior between samples studied was obtained. The degradation mechanism of the samples was studied using the integral form of the reaction model and was found that it follows the Avrami–Erofeev mechanism, but with different Avrami exponent between 1 and 3.

References

1. B. Yang, Y. Zhao, S. Wang, Y. Zhang, C. Fu, Y. Wei, L. Tao, Synthesis of multifunctional polymers through the Ugi reaction for protein conjugation, *macromolecules* **47** (2014) 5607–5612.
2. S. Fuchs, A. Pla-Quintana, S. Mazerés, A.-M. Caminade, J.-P. Majoral, Cationic and fluorescent “Janus” dendrimers. *Org. Lett.* **10**, 4751–4754 (2008)
3. J. Khandare, M. Calderon, N.-M. Dagia, R. Haag, Multifunctional dendritic polymers in nanomedicine: opportunities and challenges. *Chem. Soc. Rev.* **41**, 2824–2848 (2012)
4. S. De, A. Khan, Efficient synthesis of multifunctional polymers via thiol-epoxy “click” chemistry. *Chem. Commun.* **48**, 3130–3132 (2012)
5. M. Behl, M.Y. Razzaq, A. Lendlein, Multifunctional shape-memory polymers. *Adv. Mater.* **22**, 3388–3410 (2010)
6. I. Gadwal, A. Khan, Protecting-group-free synthesis of chain-end multifunctional polymers by combining ATRP with thiol-epoxy ‘click’ chemistry. *Polym. Chem.* **4**, 2440–2444 (2013)
7. H. Zeng, H.C. Little, T.N. Tiambeng, G.A. Williams, Z. Guan, Multifunctional dendronized peptide polymer platform for safe and effective siRNA delivery. *J. Am. Chem. Soc.* **135**, 4962–4965 (2013)
8. L. Persano, A. Camposo, D. Pisignano, Integrated bottom-up and top-down soft lithographies and microfabrication approaches to multifunctional polymers. *J. Mater. Chem. C* **1**, 7663–7680 (2013)
9. A. Hirao, M. Hayashi, S. Loykulnant, K. Sugiyama, S.W. Ryu, N. Haraguchi, A. Matsuo, T. Higashihara, Precise syntheses of chain-multi-functionalized polymers, star-branched polymers, star-linear block polymers, densely branched polymers, and dendritic branched polymers based on iterative approach using

- functionalized 1,1-diphenylethylene derivatives. *Prog. Polym. Sci.* **30**, 111–182 (2005)
- M.J. Dunlop, C. Agatemor, A.S. Abd-El-Aziz, R. Bissessur, Nanocomposites derived from molybdenum disulfide and an organoiron dendrimer. *J. Inorg. Organomet. Polym. Mater.* **27**(Suppl. 1), S84–S89 (2017)
 - S. Alaa, Abd-El-Aziz, Christian Agatemor, Emerging opportunities in the biomedical applications of dendrimers. *J. Inorg. Organomet. Polym. Mater.* **28**, 369–382 (2018)
 - M. Alsehli, S.Y. Al-Raqa, I. Kucukkaya, P.R. Shipley, B.D. Wagner, A.S. Abd-El-Aziz, Synthesis and photophysical properties of a series of novel porphyrin dendrimers containing organoiron complexes. *J. Inorg. Organomet. Polym. Mater.* **29**, 628–641 (2019)
 - S. Svenson, D.A. Tomalia, Dendrimers in biomedical applications-reflections on the field. *Adv. Drug Delivery Rev.* **64**, 102–115 (2012)
 - D.A. Tomalia, J.B. Christensen, U. Boas, *Dendrimers, Dendrons, and Dendritic Polymers: Discovery, Applications, and the Future* (Cambridge University Press, Cambridge, UK, 2012)
 - A.R. Menjoge, R.M. Kannan, D.A. Tomalia, Dendrimer-based drug and imaging conjugates: design considerations for nanomedical applications. *Drug Discovery Today* **15**, 171–185 (2010)
 - M. Samoc, J.P. Morrall, G.T. Dalton, M.P. Cifuentes, M.G. Humphrey, Two-photon and three-photon absorption in an organometallic dendrimer. *Angew. Chem. Int. Ed.* **46**, 731–733 (2007)
 - K. Onitsuka, N. Ohara, F. Takei, S. Takahashi, Organoruthenium dendrimers possessing tris(4-ethynylphenyl)amine bridges. *Organometallics* **27**, 25–27 (2007)
 - K.A. Green, M.P. Cifuentes, M. Samoc, M.G. Humphrey, Syntheses and NLO properties of metal alkynyl dendrimers. *Coord. Chem. Rev.* **255**, 2025–2038 (2011)
 - C. J. Jeffery, M. P. Cifuentes, G. T. Dalton, T. C. Corkery, M. D. Randles, A. C. Willis, M. Samoc, M. G. Humphrey, Organometallic complexes for nonlinear optics, 47 – synthesis and cubic optical nonlinearity of a stilbenylethynylruthenium dendrimer, *macromol. rapid commun.* **31** (2010) 846–849.
 - C.E. Powell, J.P. Morrall, S.A. Ward, M.P. Cifuentes, E.G. Notaras, M. Samoc, M.G. Humphrey, Dispersion of the third-order nonlinear optical properties of an organometallic dendrimer. *J. Am. Chem. Soc.* **126**, 12234–12235 (2004)
 - A.M. McDonagh, M.G. Humphrey, M. Samoc, B. Luther-Davies, Organometallic complexes for nonlinear optics: 17.1 synthesis, third-order optical nonlinearities, and two-photon absorption cross section of an alkynylruthenium dendrimer. *Organometallics* **18**, 5195–5197 (1999)
 - J. Alvarez, T. Ren, A.E. Kaifer, Redox potential selection in a new class of dendrimers containing multiple ferrocene centers. *Organometallics* **20**, 3543–3549 (2001)
 - J.R. Aranzas, C. Belin, D. Astruc, Assembly of dendrimers with redox-active [$\text{CpFe}(\mu\text{-CO})_4$] clusters at the periphery and their application to oxo-anion and adenosine-5'-triphosphate sensing. *Angew. Chem. Int. Ed.* **45**, 132–136 (2006)
 - C.M. Casado, B. González, I. Cuadrado, B. Alonso, M. Morán, J. Losada, Mixed ferrocene-cobaltocenium dendrimers. *Angew. Chem. Int. Ed.* **39**, 2135–2138 (2000)
 - R. Djeda, A. Rapakousiou, L. Liang, N. Guidolin, J. Ruiz, D. Astruc, Click syntheses of 1,2,3-triazolylbiferrocenyl dendrimers and the selective roles of the inner and outer ferrocenyl groups in the redox recognition of ATP²⁻ and Pd²⁺. *Angew. Chem. Int. Ed.* **49**, 8152–8156 (2010)
 - K. Takada, D.J. Díaz, H.D. Abruña, I. Cuadrado, B. González, C.M. Casado, B. Alonso, M. Morán, J. Losada, Cobaltocenium-functionalized poly(propylene imine) dendrimers: redox and electrogravimetric studies and AFM imaging. *Chem. Eur. J.* **7**, 1109–1117 (2001)
 - S.M. Waybright, K. McAlpine, M. Laskoski, M.D. Smith, U.H. Bunz, Organometallic dendrimers based on (tetraphenylcyclobutadiene) cyclopentadienylcobalt modules. *J. Am. Chem. Soc.* **124**, 8661–8666 (2002)
 - R. Djeda, C. Ornelas, J. Ruiz, D. Astruc, Branching the electron-reservoir complex $[\text{Fe}(\eta^5\text{-C}_5\text{H}_5)(\eta^6\text{-C}_6\text{Me}_6)][\text{PF}_6]$ onto large dendrimers: “click”, amide, and ionic bonds. *Inorg. Chem.* **49**, 6085–6101 (2010)
 - Z. Cheng, D.L. Thorek, A. Tsourkas, Gadolinium-conjugated dendrimer nanoclusters as a tumor-targeted T1 magnetic resonance imaging contrast agent. *Angew. Chem. Int. Ed.* **49**, 346–350 (2010)
 - A.J.L. Villaraza, A. Bumb, M.W. Brechbiel, Macromolecules, dendrimers, and nanomaterials in magnetic resonance imaging: the interplay between size, function, and pharmacokinetics. *Chem. Rev.* **110**, 2921–2959 (2010)
 - K. Luo, G. Liu, W. She, Q. Wang, G. Wang, B. He, H. Ai, Q. Gong, B. Song, Z. Gu, Gadolinium-labeled peptide dendrimers with controlled structures as potential magnetic resonance imaging contrast agents. *Biomaterials* **32**, 7951–7960 (2011)
 - A.S. Abd-El-Aziz, E.A. Strohm, Transition metal-containing macromolecules: En route to new functional materials. *Polymer* **53**, 4879–4921 (2012)
 - M. Ottaviani, D. Appelhans, F. J. de la Mata, S. García-Gallego, A. Fattori, C. Coppola, M. Cangiotti, L. Fiorani, J. Majoral, Caminade, in *Dendrimers in Biomedical Applications*, 1st ed., (Eds: B. Klajnert, L. Peng, V. Cefia), RSC Publishing, Cambridge, UK, 2013; p. 115.
 - Q.M. Kainz, O. Reiser, Polymer- and Dendrimer-coated magnetic nanoparticles as versatile supports for catalysts, scavengers, and reagents. *Acc. Chem. Res.* **47**, 667–977 (2014)
 - S. Vyazovkin, A.K. Burnham, J.M. Criado, L.A. Pérez-Maqueda, C. Popescu, N. Sbirrazzuoli, ICTAC kinetics committee recommendations for performing kinetic computations on thermal analysis data. *Thermochim. Acta* **520**, 1–19 (2011)
 - J. Farjas, P. Roura, Isoconversional analysis of solid-state transformations: a critical review. Part I. Single step transformations with constant activation energy. *J. Therm. Anal. Calorim.* **105**, 757–766 (2011)
 - S. Vyazovkin, K. Chrissafis, M.L. Di Lorenzo, N. Koga, M. Pijolat, B. Roduit, N. Sbirrazzuoli, J.J. Suñol, ICTAC kinetics committee recommendations for collecting experimental thermal analysis data for kinetic computations. *Thermochim. Acta* **590**, 1–23 (2014)
 - Z. Ma, J. Wang, Y. Yang, Y. Zhang, C. Zhao, Y. Yu, S. Wang, Comparison of the thermal degradation behaviors and kinetics of palm oil waste under nitrogen and air atmosphere in TGA-FTIR with a complementary use of model-free and model-fitting approaches. *J. Anal. Appl. Pyrolysis* **134**, 12–24 (2018)
 - N. Monika, V. Mulchandani, Katiyar, Generalized kinetics for thermal degradation and melt rheology for poly (lactic acid)/poly (butylene succinate)/functionalized chitosan based reactive nanobiocomposite. *Int. J. Biol. Macromol.* **141**, 831–842 (2019)
 - A.A. Joraid, R.M. Okasha, C.L. Rock, A.S. Abd-El-Aziz, A nonisothermal study of organoiron poly(alkynyl methacrylate) coordinated to dicobalt hexacarbonyl using advanced kinetics modelling. *J. Inorg. Organomet. Polym. Mater.* **24**, 121–127 (2014)
 - M. Remanan, M. Kannan, R.S. Rao, S. Bhowmik, L. Varshney, M. Abraham, K. Jayanarayanan, Microstructure development, wear characteristics and kinetics of thermal decomposition of hybrid nanocomposites based on poly aryl ether ketone, boron carbide and multi walled carbon nanotubes. *J. Inorg. Organomet. Polym. Mater.* **27**, 1649–1663 (2017)
 - S. Ebrahimi, A. Shakeri, T. Alizadeh, Thermal decomposition of ammonium perchlorate in the presence of cobalt hydroxyl@ nano-porous polyaniline, 29 (2019) 1716–1727.

43. A.A. Joraid, The effect of temperature on nonisothermal crystallization kinetics and surface structure of selenium thin films. *Phys B* **390**, 263–269 (2007)
44. A.A. Joraid, S.N. Alamri, A.A. Abu-Sehly, S.Y. Al-Raqa, P.O. Shipman, P.R. Shipley, A.S. Abd-El-Aziz, Isothermal kinetics and thermal degradation of an aryl azo dye-containing polynorbornene. *Thermochim. Acta* **515**, 38–42 (2011)
45. H.L. Friedman, Kinetics of thermal degradation of char-forming plastics from thermogravimetry: application to a phenolic plastic. *J. Polym. Sci. C* **6**, 183–195 (1964)
46. T.A. Ozawa, A new method of analyzing thermogravimetric data. *Bull. Chem. Soc. Jpn.* **38**, 1881–1886 (1965)
47. J.H. Flynn, L.A. Wall, Thermal analysis of polymer by thermogravimetric analysis. *J. Res. Natl. Bur. Stand. Sect. A* **70**, 487–523 (1966)
48. S. Vyazovkin, Evaluation of activation energy of thermally stimulated solid-state reactions under arbitrary variation of temperature. *J. Comput. Chem.* **18**, 393–402 (1997)
49. S. Vyazovkin, Modification of the integral isoconversional method to account for variation in the activation energy. *J. Comput. Chem.* **22**, 178–183 (2001)
50. S. Vyazovkin, *Isoconversional kinetics of thermally stimulated processes* (Springer International Publishing, Switzerland, 2015)
51. A.S. Abd-El-Aziz, E.K. Todd, R.M. Okasha, P.O. Shipman, T.E. Wood, Macromolecules containing redox-active neutral and cationic iron complexes. *Macromolecules* **38**(38), 9411–9419 (2005)
52. B. Roduit, Prediction of the progress of solid-state reactions under different temperature modes. *Thermochim. Acta* **388**, 377–387 (2002)
53. A.K. Burnham, L.N. Dinh, A comparison of isoconversional and model-fitting approaches to kinetic parameter estimation and application prediction. *J. Therm. Anal. Cal.* **89**, 479–490 (2007)
54. B. Roduit, L. Xia, P. Folly, B. Berger, J. Mathieu, A. Sarbach, H. Andres, M. Ramin, B. Vogelsanger, D. Spitzer, H. Moulard, D. Dilhan, The simulation of the thermal behavior of energetic materials based on DSC and HFC signals. *J. Therm. Anal. Cal.* **93**, 143–152 (2008)
55. B. Roduit, W. Dermaut, A. Lunghi, P. Folly, B. Berger, A. Sarbach, Advanced kinetics-based simulation of time to maximum rate under adiabatic conditions. *J. Therm. Anal. Cal.* **93**, 163–173 (2008)
56. A.A. Joraid, I.M.A. Alhousuni, Effect of heating rate on the kinetics and mechanism of crystallization in amorphous $\text{Se}_{85}\text{Te}_{10}\text{Pb}_5$ glasses. *Thermochim. Acta* **595**, 28–34 (2014)

Publisher's Note Springer Nature remains neutral with regard to jurisdictional claims in published maps and institutional affiliations.